HHS Public Access

Author manuscript

J Electrochem Soc. Author manuscript; available in PMC 2024 September 27.

Published in final edited form as:

J Electrochem Soc. 2023 September ; 170(9): . doi:10.1149/1945-7111/acfa68.

Characterization of Factors Affecting Stripping Voltammetry on Thermoplastic Electrodes

Catherine J McMahon,

Brandaise Martinez,

Charles S. Henry

Colorado State University, Fort Collins, Colorado 80523, USA

Abstract

Thermoplastic carbon electrodes (TPEs) are an alternative form of carbon composite electrodes that have shown excellent electrochemical performance with applications in biological sensing. However, little has been done to apply TPEs to environmental sensing, specifically heavy metal analysis. The work here focuses on lead analysis and based on their electrochemical properties, TPEs are expected to outperform other carbon composite materials; however, despite testing multiple formulations, TPEs showed inferior performance. Detailed electrode characterization was conducted to examine the cause for poor lead sensing behavior. X-Ray photoelectron spectroscopy (XPS) was used to analyze the surface functional groups, indicating that acidic and alkaline functional groups impact lead electrodeposition. Further, scanning electron microscopy (SEM) and electrochemical characterization demonstrated that both the binder and graphite can influence the surface morphology, electroactive area, and electron kinetics.

Keywords

Carbon Electrodes; Thermoplastic Electrodes; Electrochemical Sensors; Heavy Metal Analysis; Lead Analysis

1.0 Introduction

Carbon electrodes have become increasingly popular due to their wide applicability across a variety of fields. They have been utilized in batteries, fuel cells, capacitors, and chemical sensors.[1–5] Several different forms of carbon electrodes have been developed, including screen and stencil printed, glassy carbon, carbon paste, and carbon composite.[6–11] However, carbon electrodes often suffer from difficult fabrication processes and slow electron transfer kinetics in comparison to their precious metal counterparts.[12] To combat these problems, thermoplastic electrodes (TPEs) were developed. They are easily fabricated carbon composite electrodes that maintain exceptional conductivity and electron transfer kinetics.[13–20] Three primary thermoplastic binders have been explored for TPEs, including polymethyl methacrylate (PMMA),[13,21] polycaprolactone (PCL),[14,16] and polystyrene

[z] chuck.henry@colostate.edu .

(PS).[17,18] All binders create functional electrodes, but their individual properties greatly influence their application due to their unique surface and electrochemical properties. The type of carbon used has also been examined, including a variety of sized particles from 500 nm to 130 μm of naturally and synthetically sourced graphite. [13]

Previous work has demonstrated that PS and PCL electrodes can make effective biological sensors,[16,22–24] but little has been done to apply TPEs to environmental monitoring. Other types of carbon-based electrochemical sensors have been developed for a variety of environmental applications and contaminants, including soil and water analysis, pesticides, and heavy metals.[25–29] Heavy metal analysis is of particular concern due to multiple contamination sources leaching into common consumer products, including food and water.[30–32] In conjunction with anodic stripping voltammetry and other electrochemical techniques, carbon-based sensors have been able to detect heavy metals in water and soil sources at or below FDA and EPA permitted levels.[33,34] Of particular interest is the detection of lead in drinking water due to the potential health risks even at very low concentration.[35,36] However, many of these techniques require extensive surface modification, including precious metal nanoparticles, carbon nanostructures, and complex surface additives or long incubation times.[37,38] Due to the excellent electrochemical properties of TPEs, it was hypothesized that they are suitable candidates for heavy metal monitoring without the need for surface modification.

Here we characterize six different types of thermoplastic electrodes for the analysis of lead in water. Previously described binders, PMMA, PCL, and PS, are fabricated with two different carbon types (synthetic and natural), with particle size ranging from 16 μm to 130 μm, representing a spectrum of graphite used when designing carbon composite electrodes. Preliminary lead analysis indicates the use of different graphite and binders creates a broad range of surface properties which significantly influence lead metal sensing with TPEs. Several characterization techniques, including scanning electron microscopy (SEM), X-ray photoelectron spectroscopy (XPS), and electrochemical characterization were conducted to better understand the impact of the electrode material on the sensor performance. Before TPEs can be broadly applied to biological or environmental sensors, an in-depth analysis of their physical and electrochemical properties is crucial to understand the influence of fabrication materials on performance. The studies presented in this work illustrate that lead sensing is influenced by both the surface functional groups and the surface morphologies of the thermoplastic electrodes. Further, both the binder and graphite can impact electrode performance, further affecting the ability of the electrodes to be used for lead sensing.

2.0 Experimental

2.1 Chemicals and Reagents

Dichloromethane (DCM), ethyl acetate, sodium acetate and trace metal grade acetic acid were sourced from ThermoFisher Scientific (Waltham, MA, USA). Potassium ferrocyanide (≥98.5%), potassium ferricyanide (99%), potassium chloride, polystyrene 45K MW (PS), and 1000 mg/L lead and bismuth standards were sourced from Sigma Aldrich (St. Louis, MO, USA). Graphites were sourced from Asbury Carbon Mills, Inc. (Asbury, NJ, USA).

Polycaprolactone (PCL) was from ThermoMorph® (Toledo, OH, USA) and polymethyl methacrylate (PMMA) was from Fort Collins Plastics (Fort Collins, CO, USA).

2.2 Fabrication of TPEs

All TPE formulations were pressed into three-electrode systems, as shown in Schematic 1. The fabrication protocol was adapted from previous work.[13] Briefly, electrode templates (3 mm WE and RE, 5 mM CE) were designed with CorelDraw (Alludo, Ottawa, ON, Canada) then laser cut out of ¼ inch bulk extruded PMMA using a CO2 laser cutter (Epilog Laser, Golden, CO, USA). The carbon composite material was made by dissolving 1 g of thermoplastic in approximately 15 mL of DCM (PCL and PS) or ethyl acetate (PMMA) and mixing with the graphite in a 2:1, carbon:binder ratio. Graphite was either TC303 synthetic graphite (16-30 μm) or 3569 natural graphite (33-180 μm). The resulting carbon composite was pressed into the template using a manual hydraulic heat press (Carver, Inc., Wabash, IN, USA), set at 90°C with pressure between 1000-1200 psi. PCL and PS carbon composite materials were allowed to dry completely before pressing, and the PMMA material was dried to a gum-like texture before pressing. PMMA and PCL TPEs were pressed for approximately 1 hour and PS TPEs were pressed overnight to accommodate the higher melting point of PS relative to the template. Excess material was removed using wet 150 grit silicon carbide sandpaper. Solid core tinned copper wire (0.65 mm diameter) was added to each electrode using silver paint (SPI Supplies, West Chester, PA, USA) and sealed with 2-part quick set epoxy (Loctite®, Henkel Corp., Rocky Hill, CT, USA).

2.3 Electrochemical Detection of Lead

Square-wave anodic stripping voltammetry was used to deposit and evaluate Pb^{2+} on TPE surfaces. Deposition and stripping parameters were adapted from previous work.[34] Bismuth was added to sample solutions to aid in deposition by forming stable alloys with the Pb^{2+}.[39] All buffer, pH and bismuth concentrations were replicated with minor modifications to the electrochemical parameters.[34] Solutions were prepared and diluted in MilliQ water and the use of glassware was avoided for Pb^{2+} solutions. A deposition potential of −1.4V was used, with an amplitude of 40 mV and a frequency of 15 Hz. Metal solutions were deposited for 360 s. Prior to use, electrodes were polished using sequential 150, 600, and 4000 grit wet silicon carbide sandpaper and allowed to air-dry. Electrodes were then cleaned electrochemically using chronoamperometry at 0.4V for 120 s, using 100 μL of 0.1M acetate buffer, pH 4.0. All measurements used 100 μL of Pb^{2+} standards.

2.4 Cyclic Voltammetry and Electroactivity Measurements

All electrochemical measurements were performed on a PalmSens 4 potentiostat (Palmsens BV, Randhoeve 221, 2995 GA Houten, Netherlands). TPEs were polished using sequential 150, 600, and 4000 grit wet silicon carbide sandpaper before use. After sanding, arrays were sonicated in Milli-Q water for 5 minutes to remove polishing sediments, then allowed to air-dry completely. All reported potentials are referenced against a carbon pseudo-reference TPE built into the array. Ferri/ferrocyanide ($Fe(CN)_6^{3-/4-}$, 1 mM of each oxidation state) in potassium chloride (0.1 M) was used to collect cyclic voltammograms (CVs) in the positive direction from −0.4 V to 0.4 V (versus carbon pseudo-reference) at scan rates ranging from 10 mV/s – 500 mV/s in random order. Representative CVs were performed at 100 mV/s.

2.5 Surface Morphology and Composition Analysis

Single 1 mM diameter TPE models were fabricated as described above with no wires added for ease of sample manipulation. Samples were gold sputter coated (Desk II Gold Sputter Coater, Denton Vacuum, LLC., Moorestown, NJ, USA) for 15 s to a thickness of 10 nm prior to scanning electron microscopy (SEM) using a JEOL JSM-6500F field emission scanning electron microscope (JEOL, Tokyo, Japan) at 10 kV acceleration voltage. X-ray photoelectron spectroscopy (XPS) was performed using a Physical Electronics PE-5800 X-Ray Photoelectron Spectrometer (Physical Electronics, Inc., Chanhassen, MN, USA) equipped with monochromated Al anode producing Al kα x-rays, 0.8 x 0.8 mm aperture, 20 μA electron neutralizer, and argon ion gun neutralizer. The resulting spectra were processed and analyzed via CasaXPS (Casa Software Ltd.). Optical profilometry was performed on a Zemetrics ZeScope (Zygo, Middlefield, CT). Prior to each technique, the TPE models were polished, rinsed, and air-dried the same as in the electrochemical measurements.

3.0 Results and Discussion

3.1 Lead Detection on TPEs

Preliminary calibration curves were generated for all six TPE compositions for 10-200 ppb of Pb^{2+}. Seen in Figure 1, all electrode types generate a reproducible linear response in peak current as a function of Pb^{2+} concentration. Representative voltammograms at each concentration showing the well resolved peaks are available in Figure S1. The coefficient of variation ranges from 4 – 17% with the 10 ppb currents contributing the most to the variability, as expected. Across the binder types, differences in the potential of the carbon pseudo-reference electrodes cause minor shifts in the peak potential. Subsequently, the characteristics of the electrode materials likely impact the electrodeposition and subsequent stripping voltages of the Pb^{2+}. Both PMMA and PS electrodes were able to detect 10 ppb Pb^{2+}, while the PCL electrodes were only able to detect 50 ppb Pb^{2+} with good peak resolution. Overall, the peak currents for PCL electrodes are smaller in relation to both PS and PMMA. For PCL electrodes, the peak heights for the 200 ppb Pb^{2+} standard solutions are 2.5 ± 0.3 μA and 2.7 ± 0.3 μA for 3569 and TC303, respectively. For the PMMA electrodes, the 3569 graphite produces more current at 200 ppb relative to TC303, with peak heights of 7.5 ± 0.05 μA versus 5.6 ± 0.2 μA, respectively. The opposite is true of the PS electrodes with peak heights of 7.3 ± 0.1 μA and 9.5 ± 0.5 μA for 3569 and TC303, respectively. Comparing the relative peak heights across binder and graphite combinations of the six electrode types, PS-TC303 performed the best.

The sensitivities, taken as the slope of the linear fits, for each electrode type reported in Table 1 were calculated from the calibration curves seen in Figure 1. The obtained sensitivities are lower than what is observed for other carbon electrodes in the literature. For example, the sensitivity of Pb^{2+} detection from Bi-coated stencil-printed carbon electrodes (SPCEs) were 0.10 μA/ppb[34] and 0.08 μA/ppb.[40] Previous work established that TPEs are more electrochemically robust than SPCEs,[13] which makes the lower Pb^{2+} sensitivity on TPEs surprising. Thus, the need arose to examine the physical properties of the TPEs more carefully to better understand the behavior for future applications in lead, and eventually other heavy metals, sensing.

The metal deposition herein was carried out under quiescent (diffusion-only) solution conditions and was limited by mass transport of Pb^{2+} to the electrode surface. Since the same solution volumes and concentrations were tested on each TPE formulation, it suggests that the surface properties of the TPEs are influencing lead deposition. It can be speculated that a rougher surface may deposit the same, or more, Pb^{2+} ions in relation to a smoother one, but if the graphitic edge planes are more pronounced, the re-oxidation of the Pb^{2+} could be impacted through physical hinderance. Further, surface functional groups on the electrode surface can impact the Pb^{2+} electrodeposition.[41] More acidic groups, such as carboxylic acids have shown higher prevalence of Pb^{2+} deposits than surfaces without, due to an increase in adsorption sites [41]. Additionally, a high prevalence of carbonyl or alkaline functional groups hinder Pb^{2+} deposition. To better understand the surface chemistry and physical dynamics of the TPE electrodes, several surface characterization methods were applied to the system.

3.2 Surface Composition Analysis of TPEs by XPS

Depending on the graphite and binder combination, carbon composite electrodes can have different surface functional groups, leading to complex chemical interactions.[42] The binders differ in structure (Figure 2) as both PCL and PMMA are aliphatic with an ester or a carboxylic acid functional group, respectively. PS lacks oxygen functional groups and instead contains an aromatic ring.

When the electrodes are polished, the graphene sheets can become functionalized from reacting with surrounding water and oxygen, forming carboxyls, hydroxyls, and carbonyls, among others.[43] X-ray photoelectron spectroscopy (XPS) was used to determine the functional groups and their relative abundance on the electrode surfaces of each electrode type. Based on the survey spectra (Figure S2), there are only carbon and oxygen peaks present, as expected, indicating that there are no surface contaminants. The carbon (C1s) peaks were further analyzed via high resolution spectra to examine differences among TPE composition more closely.

Figure 3 shows the high-resolution spectra for C1s for all six electrodes, grouped according to binder type. Qualitative analysis indicates that both the plastic type and graphite type impact the relative functional group abundance with each binder interacting with the graphite differently, as evidenced by the different functional group peak fitting for each high-resolution spectrum. Looking at the individual relative percentage abundances for the carbon-carbon and carbon-oxygen bonding (Figure 4), this observation is further validated.

As seen by the varying degrees of the surface functional groups, the activation of the electrode surface is contingent on both the binder and graphite used. The PS electrodes are the most impacted by the size of the graphite, with PS-TC303 containing larger amounts of C-C and C-O bonds (52.8% and 36.9%, respectively) compared to PS-3569 (31.15% and 17.41%, respectively). PS-TC303 contains 10.3% of C=O and 0% of O-C=O, whereas PS-3569 contains 51.44% of C=O groups. PS-TC303 has a larger fraction of C-C bonds, suggesting that the surface is comprised mainly of basal planes. PS-3569 has a greater number of carbon-oxygen bonds (C-O and C=O), suggesting that there are more edge planes, in relation to PS-TC303. As 3569 is a larger graphite in comparison to TC303, it is

hypothesized that the TC303 carbon lattice is more ordered and contains fewer defects. Both PCL and PMMA structures contain oxygen groups, so it is not surprising that the oxygen abundance is greater than with PS TPEs. In both binder types, the C-C bond percentage is higher with TC303 than with 3569, supporting the theory that TC303 interactions with the binders produce more basal planes than 3569. The higher relative surface oxygen content for PMMA-3569 and PCL-3569 over TC303 is hypothesized to be the result of higher abundance of graphitic defects, such as zigzag-shaped edges or arm-chair edges.[44] While the binder-graphite composite used to make the TPEs is assumed to be uniform, it is possible that heterogenous layers of binder and graphite form. Therefore, the carbon lattices throughout the depth of the electrode would have varied levels of defects, impacting the carbon-oxygen bonds observed in the XPS data.

Interestingly, both the PMMA- and PCL-TPEs contain higher abundances of carbonyls than the PS electrodes whereas the PS electrodes contain the highest abundances of carboxyl groups. As noted previously, carbonyl groups can have a negative impact on Pb^{2+} deposition and carboxyl groups can enhance deposition.[41] For the smaller graphite size (TC303), the abundance of carbonyl groups on the surface appears to have a negative impact on the Pb^{2+} sensitivity, whereas the trend is not obvious for the larger graphite, 3569. All three electrode formulations have higher levels of oxygen-containing functional groups compared to C-C for 3569 than TC303, suggesting there are more surface defects, or edge planes. Furthermore, the sensitivities for PS and PMMA Pb^{2+} deposition are similar (0.038 ± 0.001 and 0.039 ± 0.002, respectively) for 3569 ($p>0.1$), with the PS electrode containing no carbonyl groups. This suggests that in addition to the carbonyl groups, the morphology of the graphitic defects can greatly affect the deposition and subsequent stripping of Pb^{2+} at the electrode surface. Scanning electron microscopy was used to further investigate the electrode surface microstructure.

3.3 SEM Characterization

Scanning electron microscopy (SEM) images were taken of all six TPE formulations and are shown in Figure 5 (additional magnifications are available in Figure S3). For all TPE types, there is varying degrees of surface topography with heterogeneous surfaces with pockets of randomly orientated graphitic material. For the TC303 TPEs, PS has the lowest amount of edge planes, and is primarily composed of basal planes, as evidenced by the densely packed smooth surface. There are also some smaller translucent edge planes, which could resemble graphene-like behavior. The surface roughness (Rq), determined via optical profilometry, can be correlated to the presence of edge planes (Figure 6). Further, the PS has the most uniform conductive surface, evidenced by the minimal pockets of charged material. The PMMA and PCL topographies have more ridge-like defects, which can be attributed to graphitic edge planes, but could also be a result of pockets of free binder. This is particularly the case for the PCL electrodes, where the long tubular like structures seen in both graphite images are likely bulk binder material that was not well blended with the graphite powder. For the 3569 graphite, all three binders have heterogeneous pockets of graphitic material, consisting of both basal and edge planes. The PCL-3569 surface appears more densely packed, indicating the bulk material is likely more homogeneous than the TC303 material. PS-3569 has more surface roughness in relation to PS-TC303, with more pronounced edge

planes. The PMMA surfaces appear to be similar across the two graphites, with pockets of smooth and ridge-like graphitic material.

For Pb^{2+} deposition, PMMA-3569 was superior to PMMA-TC303 when comparing the sensitivities (0.039 ± 0.002 and 0.029 ± 0.001, respectively). Relating to the surface characteristics, PMMA-3569 appears to have less defects than PMMA-TC303. However, for the PS electrodes, PS-TC303 slightly outperforms PS-3569, despite the sensitivities being similar (0.050 ± 0.001 and 0.038 ± 0.001, respectively). For PS-TC303, the 200-ppb peak height is 2.2 μA higher than PS-3569. This leads to the conclusion that the size of the graphite is an important consideration when adapting the TPEs for various applications, and, in this case, lead sensing. For the PCL TPEs, both graphites had similar sensitivities (0.015 ± 0.001 and 0.013 ± 0.001), and the two graphites seem to produce similar surface morphologies with a mix of basal and edge planes. The PCL TPEs have the most bulk binder material observed in the SEM images, particularly PCL-TC303. This suggests that the PCL binder produces the least homogeneous carbon composite material, which can have direct impacts on electrode function.

3.4 Electrochemical Characterization of the TPE material

As evidenced by the XPS and SEM analysis of the TPE material, the formulation can impact both electrode surface morphology and chemistry. As seen with XPS, the surface functional groups generated by activating the carbon composite material when polishing is contingent on both the graphite and binder used. Additionally, both the graphite and binder can influence the degree and morphology of the surface defects, as evidenced by the SEM. However, all six formulations still underperform in relation to other carbon-based electrodes for Pb^{2+} analysis. Therefore, electrochemical characterization was also explored, to help understand if the different binder-graphite formulations impact electron transfer kinetics and active surface area.

All TPE formulations were evaluated using the reversible redox couple ferri/ferrocyanide, shown in Figure 7. PS-T303 TPEs showed the highest oxidative current density (420 ± 10 μA/cm^2) compared to PMMA-TC303 (310 ± 40 μA/cm^2) and PCL-TC303 (200 ± 10 μA/cm^2). For the 3569 graphite, the PS- and PMMA- oxidative current densities were not significantly different (430 ± 30 μA/cm^2 and 410 ± 20 μA/cm^2, respectively) but were roughly 2x higher than PCL (210 ± 20 μA/cm^2). Ferri/ferrocyanide is sensitive to surface oxides, so the differences in the current densities can be attributed to the different surface roughness and the surface functional groups of each of the TPEs.[45] ΔE values were also calculated for each TPE formulation. For the TC303 graphite, PS- and PMMA- electrodes were not statistically different, with ΔE values of 82 ± 4 mV and 86 ± 13 mV, respectively, indicating that both formulations have similar electron transfer kinetics. However, the PCL TPE had a much higher ΔE value of 307 ± 21 mV, suggesting that PCL can hinder electron transfer kinetics. A similar trend is observed for 3569 graphite, with ΔE values corresponding to 101 ± 15, mV 94 ± 7 mV, and 237 ± 25 mV for PS, PMMA, and PCL TPEs, respectively. Graphite appears to have a minor effect on electron transfer kinetics in PS and PMMA electrodes. On the contrary, for PCL, the TC303 graphite has ΔE 77% higher than 3569, suggesting PCL is more compatible with larger graphite particles. With PCL

having the lowest current density and high ΔE values in comparison to the PS- and PMMA-TPEs, the PCL formulations are not suitable for applications requiring surface modification, whereas the PS and PMMA are promising candidates.

To investigate the kinetics further, the heterogeneous electron transfer rate constants, k_0, was calculated for each TPE formulation using the Nicholson method.[46] Equation 1 was used, where φ is the average of the ΔE of the ferri/ferrocyanide peaks for each scan rate, D is the diffusion coefficient, F is Faraday's constant, R is the ideal gas constant, v is the scan rate, n is the number of electrons exchanged, and T is temperature (assumed 25°C).

$$\varphi = k_0[\frac{\pi DnFv}{RT}]^{-\frac{1}{2}} \quad \text{Equation 1}$$

The rate constants are shown in Table 2. The rate constants for PS- and PMMA-TPEs are similar and are comparable to glassy carbon composite electrodes (k_0 =0.005 cm·s^{-1}).[47] For the PMMA-TPEs, the graphite does not appear to have a large impact on the electron transfer kinetics, as the rate constants for TC303 and 3569 differ by 0.2 cm·s^{-1}. The size of the graphite does appear to influence the PS-TPEs, with the smaller graphite (TC303) being preferable over 3569, as the rate constant is 1 cm·s^{-1} higher for TC303 than 3569. The PCL rate constants are smaller by an order of magnitude and can only be estimated, as the high resistance of the electrodes adds error to the calculation, and the peak currents could be masked by non-Faradaic effects [46]. Further, the ΔE values for PCL-TPEs exceeded 200 mV for some scan rates, which prevents accurate determination of k_0. For both PS and PMMA, the rate constants follow the same trend as the current density, where neither graphite has a substantial impact on the PMMA TPEs, and the smaller graphite particles is preferable for PS. This suggests that the size and orientation of the binder can impact the TPE performance.

To further compare the electrodes, the electroactive surface area was calculated (Table 3). Using ferri/ferrocyanide as the redox probe, cyclic voltammograms at nine different scan rates were collected. The electroactive area was calculated using the Randles-Sevcik equation (Equation 2), where i_p is the peak current (A), n is the number of electrons transferred in the reaction, A is the electroactive surface area (cm^2), D is the diffusion coefficient (cm^2·s^{-1}), C is the concentration (M), and v is the scan rate (V·s^{-1}).[48] The diffusion coefficients used were 7.20×10^{-6} cm^2/s (reduced) and 6.66×10^{-6} cm^2/s (oxidized) [49].

$$i_p = 2.69 \times 10^5 AD^{\frac{1}{2}}Cv^{\frac{1}{2}} \quad \text{Equation 2}$$

The square root of the scan rates versus the peak currents were fit with a linear regression model (Figure 8), and the slope was used to solve for the electroactive area in Equation 2. The temperature was assumed to be 25°C. The electroactive areas for all TPE formulations are reported in Table 3.

The oxidized and reduced electroactive areas are in good agreement across all TPE formulations, with PCL having the greatest discrepancy, likely a result of redox species adsorbing to the surface and/or slow electron transfer kinetics.[45] The geometric surface area of the working electrodes (WE) for all TPE formulations was 0.071 cm^2. For the TC303 graphite, the PMMA- and PS-TPEs electroactive area were 192% and 280% greater than the geometric surface area. For the 3569 graphite, the PMMA- and PS-TPEs electroactive area were 256% and 264% greater than the geometric surface area. These values are reasonable, based on the rough surfaces (increasing electroactive surface area) observed via SEM and profilometry. The electroactive area calculations are also in good agreement with the current densities and electron transfer kinetics. For the PCL-TPEs, the electroactive surface area is smaller than the geometric surface area, which is further supported by the more resistive cyclic voltammograms in Figure 7.

4.0 Conclusions

When considering TPEs for sensing applications, it is crucial to consider binder and graphite compositions based on their chemical and physical properties. The inherent physical and chemical properties influence the utility of the electrode, in this case, for the analysis of Pb^{2+}. Despite superior electrochemical performance of TPEs over other popular carbon composite electrodes, TPEs tend to lack sensitivity for lead analysis via anodic stripping voltammetry. After thorough surface and electrochemical characterization, it was found that PS-based TPEs showed the best overall performance for both lead deposition and electrochemical characterization. However, the size of the graphite played a critical role, as PS-TC303 outperformed PS-3569. For the PS-TPEs, it is hypothesized that the aromatic group of polystyrene is responsible for creating edge planes during polishing. The orientation of the binder can create small perpendicular edge planes, allowing the material to be more densely packed, which improves electron transfer kinetics while maintaining a relatively smooth surface. PCL is likely being degraded either during fabrication and/or through polishing.[50] The hydrolysis of the binder could result in the formation of the other functional groups, mainly carbonyl groups, by reacting with the surrounding water and oxygen. Further, the long carbon chain of PCL is likely contributing to the flexibility of the binder, creating the tubular shapes observed in the SEM images. PMMA and PS are notably more brittle than PCL, likely creating more sheered edges within the graphite. PMMA has fewer surface oxides in comparison to PS, which is supported by the lower current density. Because of the carboxyl groups of the binder itself, hydrogen bonding can occur between the binder molecules, inhibiting graphite interaction with the binder, creating less densely packed conductive material. It is hypothesized that the material contains small islands of PMMA bound to itself, which could be confirmed with more extensive XPS mapping. Broadly, TPEs can be used as a screening tool for high levels of lead with no additional surface modifications needed. Further, they can be used for other heavy metals by properly selecting the graphite and polymer constituents.

Supplementary Material

Refer to Web version on PubMed Central for supplementary material.

Acknowledgements

The authors wish to thank the Analytical Resources Core (RRID: SCR 021758) at Colorado State University for instrument access, training, and assistance with sample analysis. The authors also thank NIH R01EB031510 for supporting B. Martinez and C. Henry.

References

1. Uslu B and Ozkan SA, Anal. Lett, 40, 817–853 (2007).
2. Zhang T and Ran F, Adv. Fimct. Mater, 31, 2010041 (2021).
3. Wring SA and Hart JP, Analyst, 117, 1215–1229 (1992).
4. Dubey R and Guruviah V, Ionics, 25, 1419–1445 (2019).
5. Casanova A, Iniesta J, and Gomis-Berenguer A, Analyst, 147, 767–783 (2022). [PubMed: 35107446]
6. Dekanski A, Stevanović J, Stevanović R, Nikolić BŽ, and Jovanović VM, Carbon, 39, 1195–1205 (2001).
7. Van der Linden WE and Dieker JW, Anal. Chim. Acta, 119, 1–24 (1980).
8. Kava AA and Henry CS, Talanta, 221, 121553 (2021). [PubMed: 33076109]
9. Wring SA and Hart JP, Analyst, 117, 1281–1286 (1992).
10. Švancara I, Vytras K, Kalcher K, Walcarius A, and Wang J, Electroanalysis, 21, 7–28 (2009).
11. Ramírez-García S, Alegret S, Céspedes F, and Forster RJ, Analyst, 127, 1512–1519 (2002). [PubMed: 12475044]
12. Tan S et al., Phys. Chen. Chen. Phys, 19, 8726–8734 (2017).
13. Klunder KJ, Nilsson Z, Sambur JB, and Henry CS, ACS Publ. (2017) 10.1021/jacs.7b06173.
14. Klunder KJ et al., Lab. Chip, 19, 2589–2597 (2019). [PubMed: 31250868]
15. Noviana E, Klunder KJ, Channon RB, and Henry CS, Anal. Chem, 91, 2431–2438 (2019). [PubMed: 30623637]
16. Clark KM and Henry CS, Electroanalysis, 34, 1869–1876 (2022).
17. McCord CP, Summers B, and Henry CS, ChemElectroChem, 9, e202101600 (2022).
18. McCord CP, Summers B, and Henry CS, Electrochimica Acta, 393, 139069 (2021).
19. Berg KE, Leroux YR, Hapiot P, and Henry CS, Anal. Chem, 93, 1304–1309 (2021). [PubMed: 33373524]
20. Berg KE, Leroux YR, Hapiot P, and Henry CS, ChemElectroChem, 6, 4811–4816 (2019).
21. Pradela-Filho LA, Araújo DAG, Takeuchi RM, Santos AL, and Henry CS, Anal. Chim. Acta, 1147, 116–123 (2021). [PubMed: 33485570]
22. Ozer T and Henry CS, Electrochimica Acta, 404, 139762 (2022).
23. Ozer T and Henry CS, Microchim. Acta, 189, 152 (2022).
24. Ozer T, McCord C, Geiss BJ, Dandy D, and Henry CS, J. Electrochem. Soc, 168, 047509 (2021).
25. Barton J et al., Microchim. Acta, 183, 503–517 (2016).
26. Wang J et al., Anal. Chim. Acta, 347, 1–8 (1997).
27. Shetti NP et al., Microchem. J, 149, 103976 (2019).
28. Hwang J-H et al., Sens. Actuators B Chem, 294, 89–97 (2019).
29. Manisankar P, Sundari PLA, Sasikumar R, and Palaniappan SP, Talanta, 76, 1022–1028 (2008). [PubMed: 18761149]
30. Ahmed M, Matsumoto M, and Kurosawa K, Int. J. Environ. Res, 12, 531–542 (2018).
31. Bobaker AM, Alakili I, Sarmani SB, Al-Ansari N, and Yaseen ZM, Int. J. Environ. Res. Public. Health, 16 (2019) https://www.ncbi.nlm.nih.gov/pmc/articles/PMC6603917/.
32. Fashola MO, Ngole-Jeme VM, and Babalola OO, Int. J. Environ. Res. Public. Health, 13 (2016) https://europepmc.org/articles/PMC5129257/.
33. Borrill AJ, Reily NE, and Macpherson JV, Analyst, 144, 6834–6849 (2019). [PubMed: 31657380]

34. Kava AA, Beardsley C, Hofstetter J, and Henry CS, Anal. Chim. Acta, 1103, 58–66 (2020). [PubMed: 32081189]
35. Goyer RA, Environ. Health Perspect, 100, 177–187 (1993). [PubMed: 8354166]
36. Canada H, (2016) https://www.canada.ca/en/health-canada/programs/consultation-lead-drinking-water.html.
37. Bansod B, Kumar T, Thakur R, Rana S, and Singh I, Biosens. Bioelectron, 94, 443–455 (2017). [PubMed: 28340464]
38. Yantasee W et al., Environ. Health Perspect, 115, 1683–1690 (2007). [PubMed: 18087583]
39. Wang J, Lu J, Hocevar SB, Farias PAM, and Ogorevc B, Anal. Chem, 72, 3218–3222 (2000). [PubMed: 10939390]
40. Martín-Yerga D, Álvarez-Martos I, Blanco-López MC, Henry CS, and Fernández-Abedul MT, Anal. Chim. Acta, 981, 24–33 (2017). [PubMed: 28693726]
41. Wang L et al., Electrochimica Acta, 186, 654–663 (2015).
42. Oliveira LS et al., J. Electroanal. Chem, 818, 106–113 (2018).
43. Eng AYS, Chua CK, and Pumera M, Nanoscale, 7, 20256–20266 (2015). [PubMed: 26579848]
44. Kim J et al., ACS Omega, 3, 17789–17796 (2018). [PubMed: 31458375]
45. Ji X, Banks CE, Crossley A, and Compton RG, ChemPhysChem, 7, 1337–1344 (2006). [PubMed: 16671130]
46. Randviir EP, Electrochimica Acta, 286, 179–186 (2018).
47. McCreery RL, Chem. Rev, 108, 2646–2687 (2008). [PubMed: 18557655]
48. Zhu P and Zhao Y, Mater. Chem. Phys, 233, 60–67 (2019).
49. Moldenhauer J, Meier M, and Paul DW, J. Electrochem. Soc, 163, H672 (2016).
50. Gross RA and Kalra B, Science, 297, 803–807 (2002). [PubMed: 12161646]

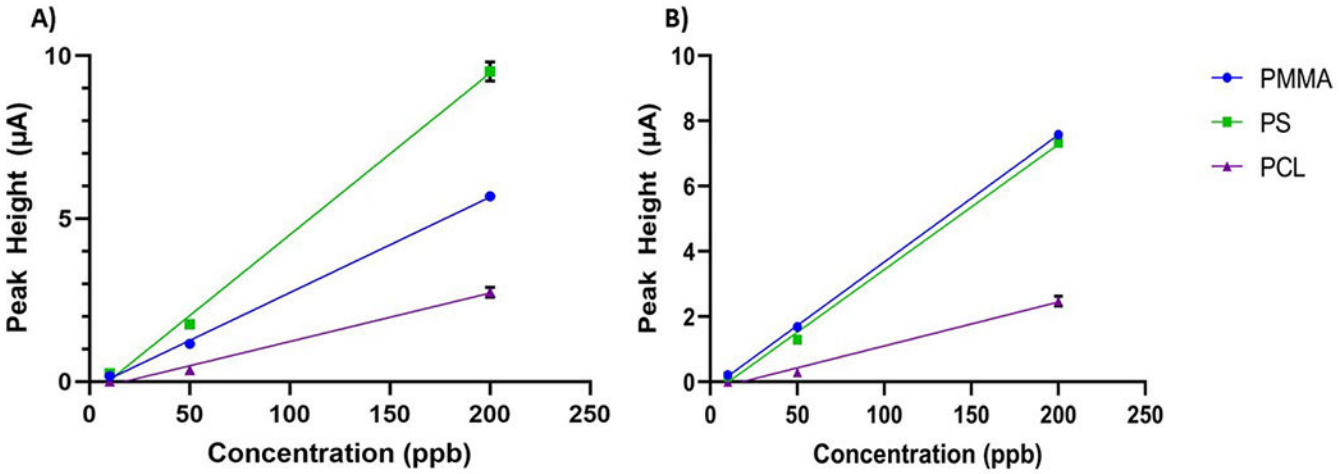

Figure 1.

Calibration curves for 10 – 200 ppb Pb^{2+} for all six TPE formulations, with 2 ppm of Bi. Analysis was performed in 0.1M acetate buffer, pH 4, 360s deposition time, −1.4V deposition potential. A) PCL-, PS-, and PMMA-3569 TPE (n=3) peak currents fit to a linear regression model. B) PCL-, PS, and PMMA-TC303 TPE (n=3) peak currents fit to a linear regression model.

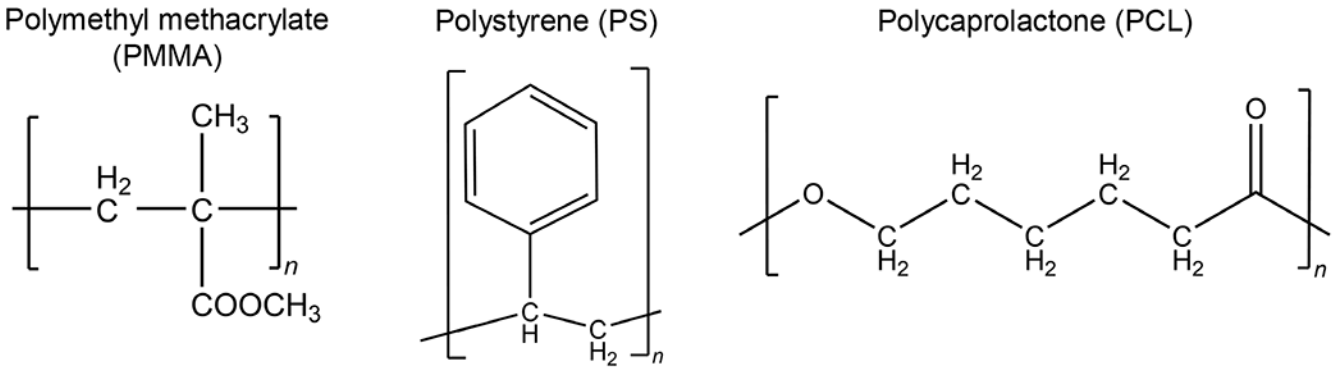

Figure 2.
Chemical structures of PMMA, PS, and PCL, given in order from left to right.

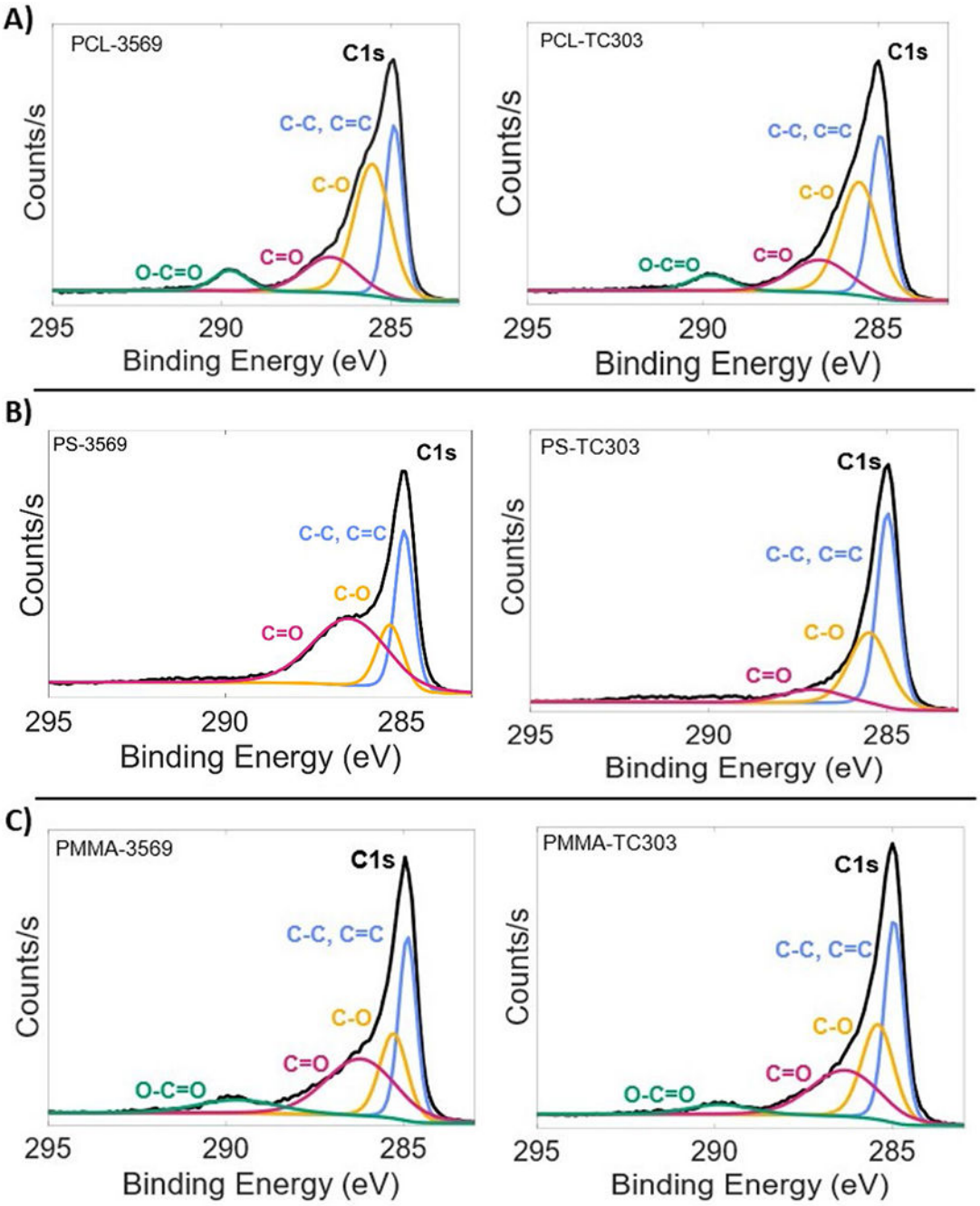

Figure 3:

X-ray photoelectron spectroscopy high resolution C1s spectra for A) PCL TPEs, B) PS-TPEs, and C) PMMA-TPEs. Spectra were fitted with CasaXPS software.

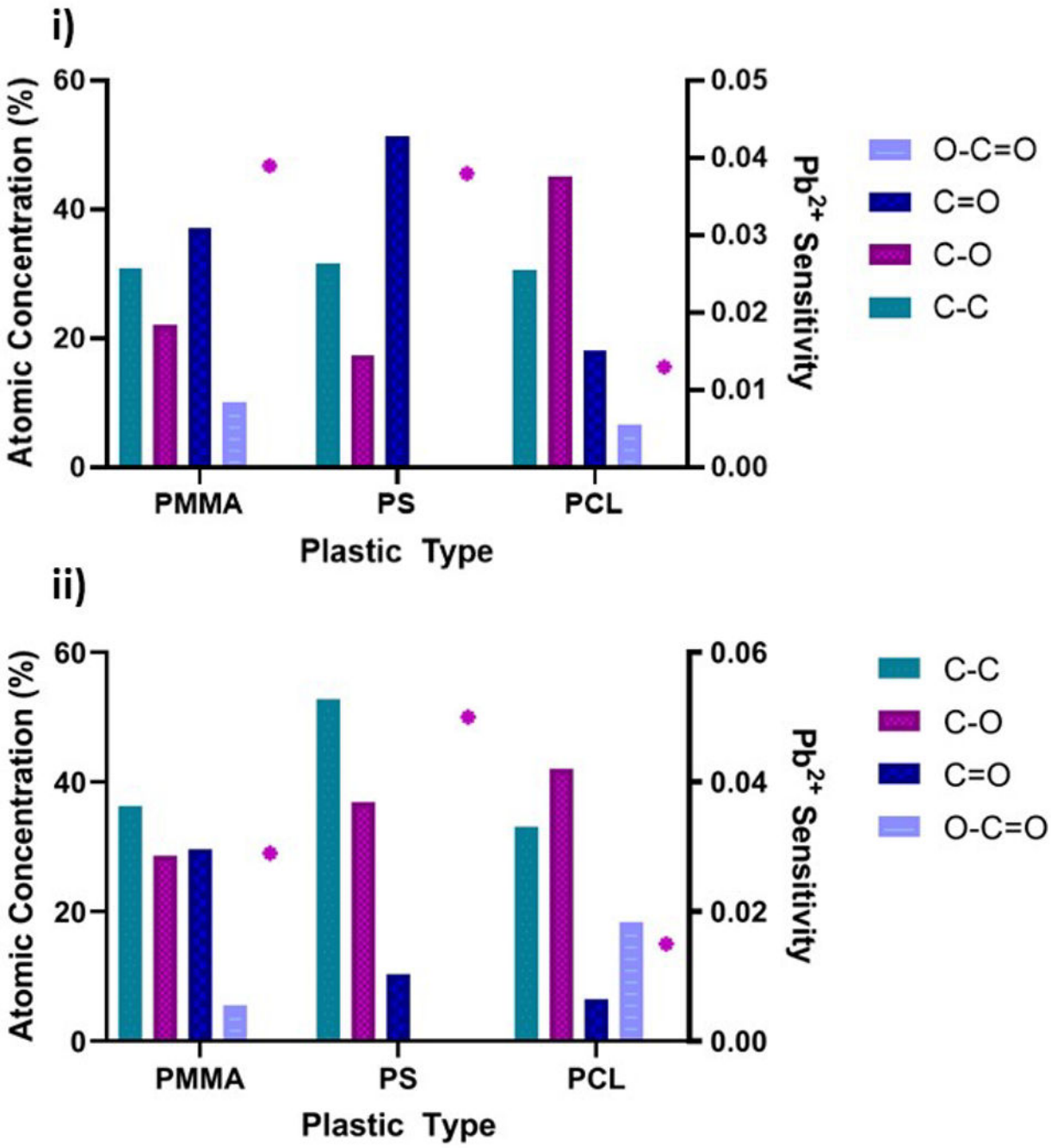

Figure 4.

Atomic concentration percentages from high resolution XPS spectra for PCL-, PS-, and PMMA-TPEs plotted against the sensitivity of the Pb^{2+} deposition, represented by the pink star for **i)** 3569 graphite and **ii)** TC303 graphite.

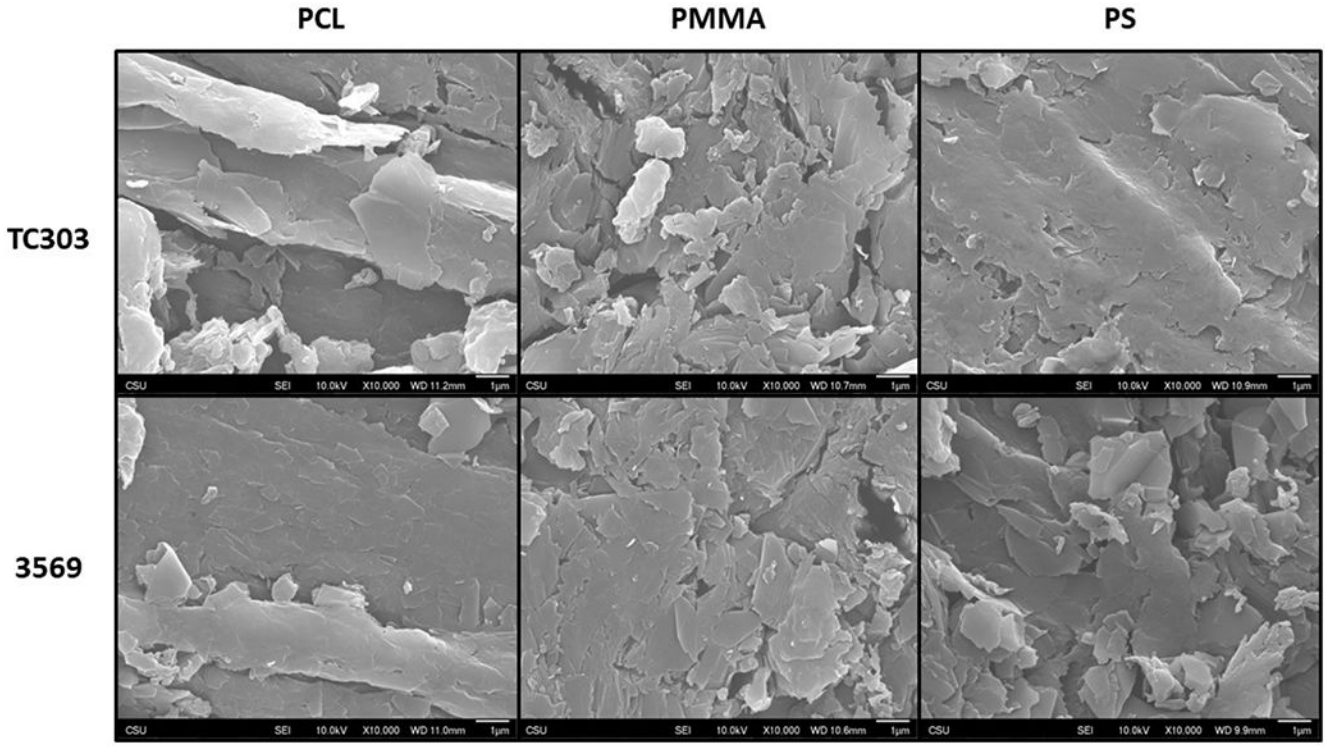

Figure 5:
SEM micrographs at 1×10^4x magnification of PCL-, PMMA-, and PS-based TPE material with TC303 graphite (top) and 3569 graphite (bottom).

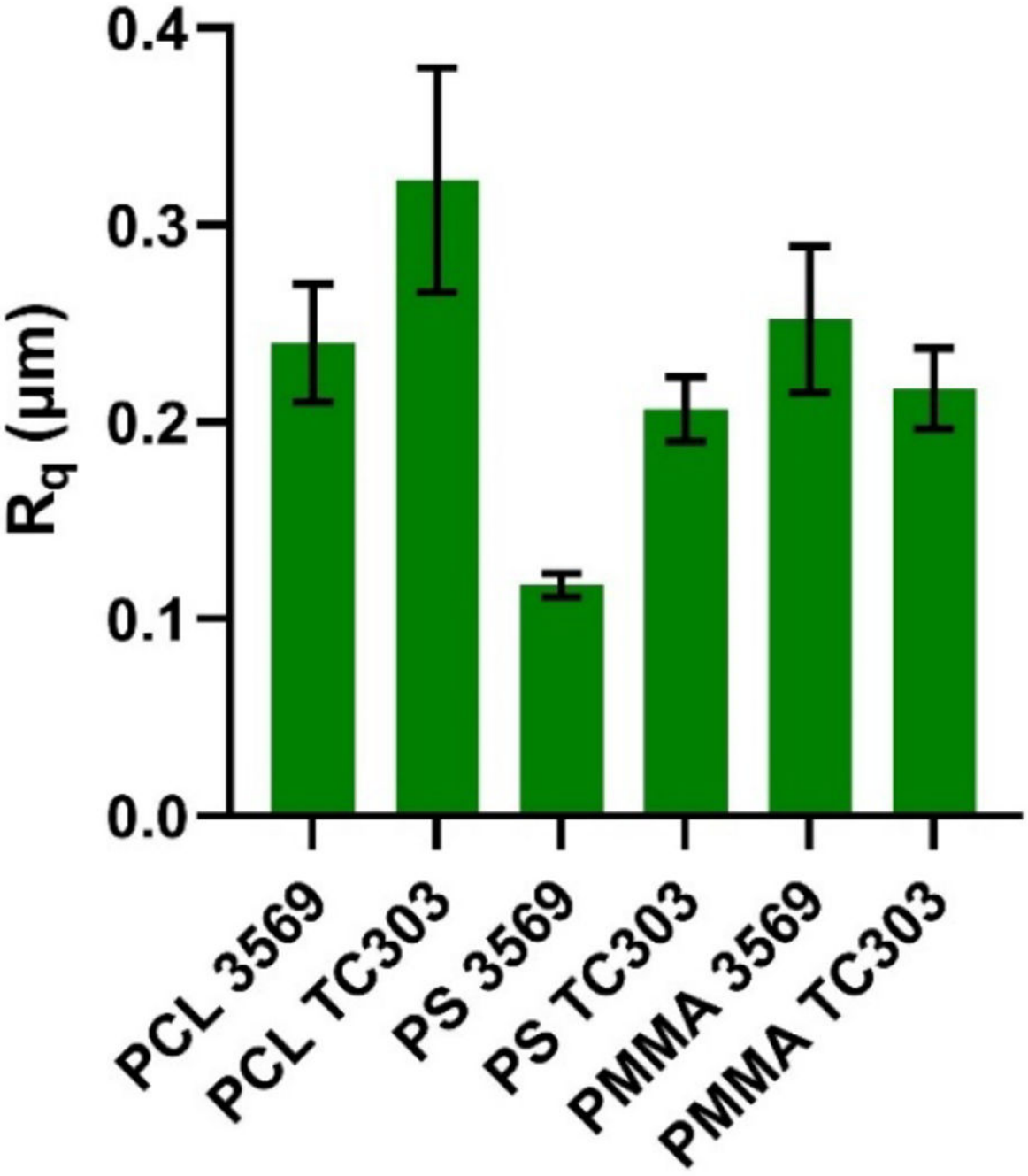

Figure 6.
Average surface roughness (R_q) (n=3) of each TPE type. Error bars represent standard deviation.

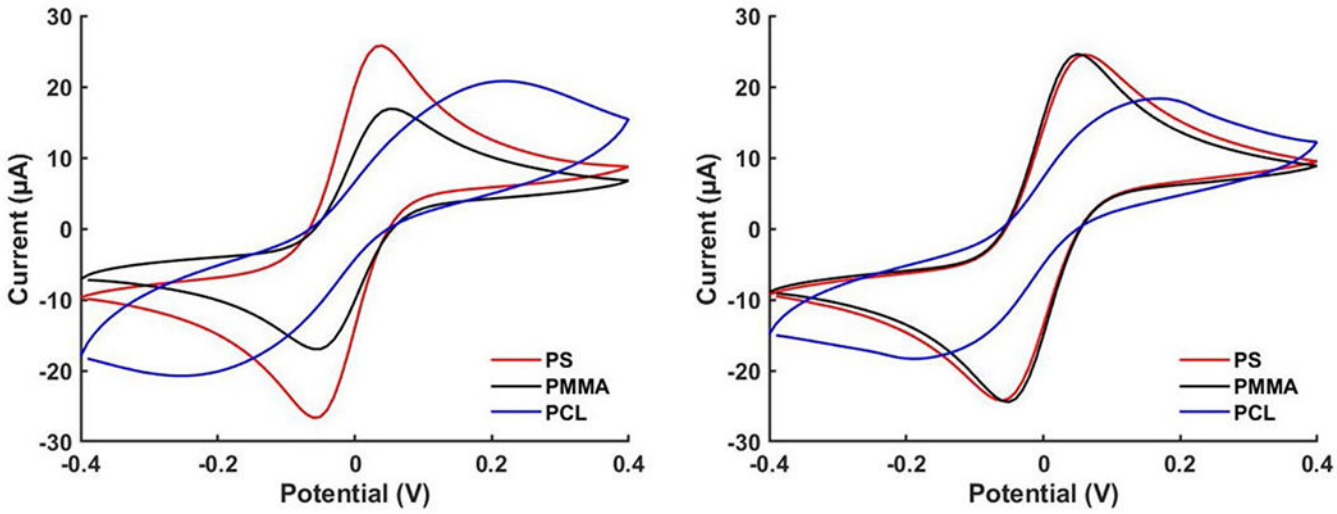

Figure 7.

Representative CVs (n=3) in 1 mM $Fe(CN)6^{3-/4-}$ in 0.1 M KCl at scan rate of 100 mV/s for PS-, PMMA-, and PCL-TPEs with TC303 graphite (left) and 3569 graphite (right).

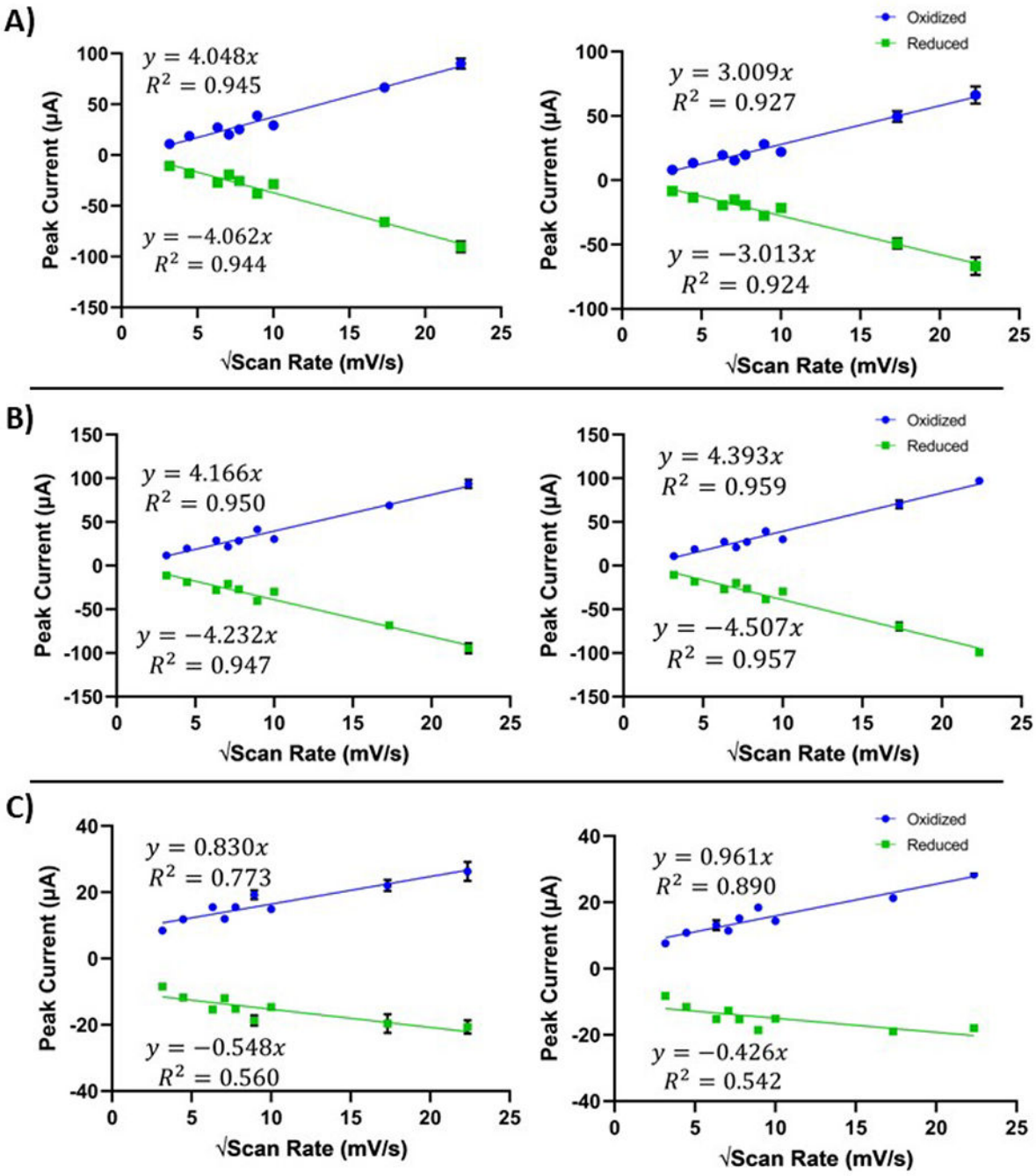

Figure 8.

Plots of the peak current vs the square root the scan rate for the oxidized and reduced peaks for **A)** PMMA-TPEs with 3569 (left) and TC303 (right), **B)** PS-TPEs with 3569 (left) and TC303 (right), and **C)** PCL-TPEs with 3569 (left) and TC303 (right).

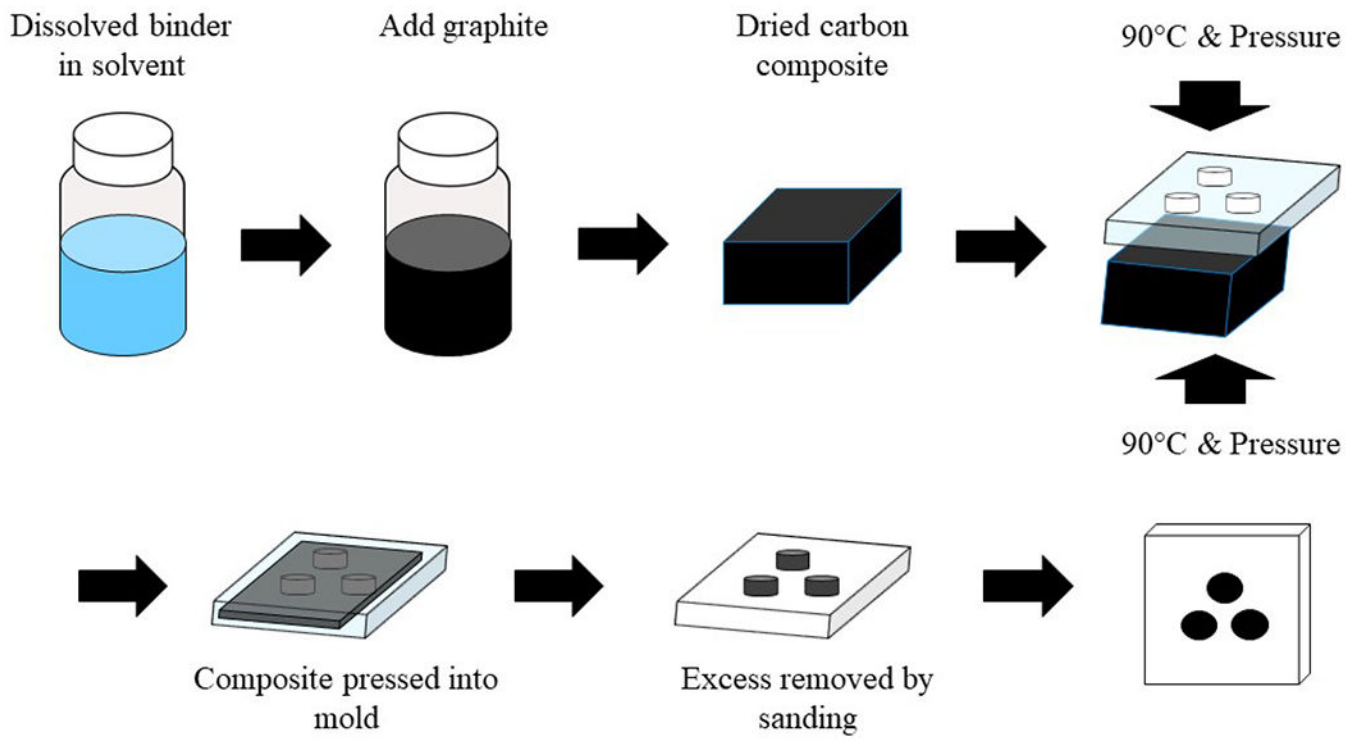

Schematic 1:
Fabrication of the thermoplastic electrodes as adapted from Klunder et al. 2017.

Table 1:

The sensitivity and the R^2 values were calculated from the calibration curve for all six TPE formulations using a linear regression model, where the sensitivity is the slope of the line. Standard deviations were calculated from triplicate runs (n=3).

	TC303			**3569**		
	PMMA	**PS**	**PCL**	**PMMA**	**PS**	**PCL**
Sensitivity (μA/ppb)	0.029 ± 0.001	0.050 ± 0.001	0.015 ± 0.001	0.039 ± 0.002	0.038 ± 0.001	0.013 ± 0.001
R^2 Value	0.997	0.994	0.982	0.999	0.996	0.979

Table 2:

Electrochemical rate constants, k_0, of 1 mM $Fe(CN)_6^{3-/4-}$ in 0.1 M KCl in relation to differing electrode formulations. The rate constants were determined from the slopes of the linear regression lines and the error shown is the standard error of the slope.

	TC303			3569		
	PMMA	**PS**	**PCL**	**PMMA**	**PS**	**PCL**
k_0(x10^{-3} cm·S^{-1})	5.1±0.1	4.6±0.5	0.94±0.06	4.9±0.7	3.6±0.9	0.84±0.01

Table 3:

Calculated electroactive areas for all binder formulations for TC303 graphite and 3569 graphite.

	TC303			3569		
	PMMA	**PS**	**PCL**	**PMMA**	**PS**	**PCL**
Oxidized (cm^2)	0.139	0.201	0.044	0.185	0.190	0.038
Reduced (cm^2)	0.133	0.197	0.019	0.178	0.185	0.024